Journal Pre-proof

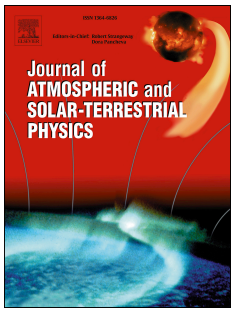

Distinguishing different lightning events based on wavelet packet transform of magnetic field signals

Shiye Huang, Weiqi Kong, Jing Yang, Qilin Zhang, Nianpeng Yao, Bingzhe Dai, Jiaying Gu

PII: S1364-6826(20)30280-7

DOI: https://doi.org/10.1016/j.jastp.2020.105477

Reference: ATP 105477

To appear in: *Journal of Atmospheric and Solar-Terrestrial Physics*

Received Date: 10 May 2020

Revised Date: 14 October 2020

Accepted Date: 14 October 2020

Please cite this article as: Huang, S., Kong, W., Yang, J., Zhang, Q., Yao, N., Dai, B., Gu, J., Distinguishing different lightning events based on wavelet packet transform of magnetic field signals, *Journal of Atmospheric and Solar-Terrestrial Physics* (2020), doi: https://doi.org/10.1016/j.jastp.2020.105477.

Distinguishing Different Lightning Events Based On Wavelet Packet Transform of Magnetic Field Signals

Shiye Huang[a], Weiqi Kong[a], Jing Yang[a,*] , Qilin Zhang[a], Nianpeng Yao[a], Bingzhe Dai[a], Jiaying Gu[a]

a. Key Laboratory of Meteorological Disaster, Ministry of Education (KLME)/ Joint International Research Laboratory of Climate and Environment Change (ILCEC)/Collaborative Innovation Center on Forecast and Evaluation of Meteorological Disasters (CIC-FEMD)/ Key Laboratory for Aerosol-Cloud-Precipitation of China Meteorological Administration, Nanjing University of Information Science & Technology, Nanjing 210044, China;

*Corresponding author: Jing Yang (jing.yang@nuist.edu.cn)

Abstract:

In this paper, the wavelet packet transform (WPT) is applied to analyze the time-frequency features of three kinds of lightning events (the cloud pulse, the return stroke and the stepped leader) and a new identification method based on WPT is proposed. The magnetic-field data used in this paper were recorded by Nanjing Lightning Location Network in 2018. Firstly, the wavelet spectra of three typical lightning events are given and it is found that spectral ranges of these three events are different. The predominant radiation frequency of the stepped leader is the highest and that of the return strokes is the lowest. A total of 232 cloud pulses, 876 return strokes and 373 stepped leaders are analyzed by WPT in order to investigate their behavior in time-frequency domain. The statistical result shows that the cloud pulse, return stroke and stepped leader radiate predominantly in the frequency range 9~56 kHz, 2~14 kHz and 52~236 kHz, respectively. According to the energy distribution characteristics, three indices are proposed to distinguish the different lightning events. It is found that the recognition rate of return stroke is 91% and that of stepped leader is up to 93%.

Key words: Wavelet packet transform, Energy spectra, Identification index, Lightning detection

1 Introduction

Lightning is a high-transient electrical discharge between two opposite charge regions in the atmosphere or ground. This discharge causes electromagnetic radiation in a wide spectrum range varying from VLF (Very Low Frequency) to VHF (Very High Frequency) (Miranda et al., 2003). There are three main kinds of lightning and they are classified by where they occur: intra-cloud (IC) lightning, cloud to cloud (CC) lightning, and cloud to ground (CG) lightning (Maggio, 2009). The discharge that occurs between two charged areas in the same cloud is called intra-cloud (IC) lightning. Cloud-to-cloud (CC) discharge occurs between two charged areas that belongs to two separate clouds (Dwyer and Uman, 2014). Cloud-to-ground (CG) lightning, which is composed of various discharge processes, starts in a thundercloud and develops down

towards the ground. The most powerful discharge process of CG lightning is return stroke, which is initiated by a downward-moving stepped leader from the cloud and an upward-moving streamer form the ground. When the downward leader approaches the ground, the strong electric field of its head causes one or several upward connection leaders at the tips of objects on the ground. The downward leader connects to one or several connecting leaders at tens to hundreds of meters above the object. At the same time, a very strong and instantaneous discharge occurs due to the huge potential difference between the downward leader and the upward connection leader. And the current continues to travel upward along the previously ionized leader channel, this is the first return stroke. If enough charges could be generated at the top of the channel in a short time, a dart leader may move down and cause a subsequent return stroke (Qie et al., 2013).

Lightning could cause great damages by the direct impacts of heating from heavy current and the indirect impacts of the induced voltages. If the heavy current and shock waves generated by lightning strike people, the heart and other vital organs will be severely damaged. What's more, Lightning is the major cause of interruptions and breakdowns for the electronic systems (Weidman et al., 1986) and high voltage transmission lines (Salimi, 2013). In addition, although lightning does not strike directly, its induced overvoltage can enter buildings through power lines, results in great damage to lines and equipment, and sometimes even fire. Due to the great disasters caused by lightning, it is very important to understand the physical essence of lightning. The electromagnetic radiation field is one of the most significant tools to understand lightning phenomena and the frequency spectrum is important for revealing the physical essence of lightning.

Two methods have been employed to measure lightning spectra (Le Vine, 1987). One technique is to measure the average and peak spectral amplitudes at a frequency directly using narrow band receivers tuned to the frequency of interest. One disadvantage of this technique is that for HF or higher frequencies, the measurements are highly variable and any specific lightning process cannot be identified (Willet et al., 1990). In the other technique, the spectrum is obtained from the electric field waveform using Fourier transform (FT). The main process is as follows: the electric field waveform is recorded by wide bandwidth devices, and the lightning spectrum is obtained from lightning radiation waveform through the fast Fourier transform (FFT). This technique requires wide bandwidth devices with huge dynamic range because the power at high frequencies decrease rapidly with frequency.

Fourier transform is a powerful tool widely used to convert stationary signals from time domain to frequency domain. One of the earliest applications of the FT was made by Watt and Maxwell (1957). In that research, FT was employed for electric field waveforms to form a composite spectrum. Fourier transform was widely used in the field of lightning after Serhan et al. (1980), they distinguished first and subsequent return stroke waveforms and calculated spectra separately. However, FT is not suitable for dealing with the transient signals, such as the lightning electromagnetic field, because time information is lost. For instance, FT can only give amplitude spectrum, but cannot show time-frequency characteristics for non-stationary signals.

The Wavelet transform (WT) is a relatively new method, which can show properties simultaneously in frequency and time domain. The WT has advantage over the FT as it could decompose a signal in time-frequency space, which allows to study each frequency component with appropriate time resolution (Issac et. al.,2004). Additionally, it can be used to determine the dominant modes and how their change over time (Torrence and Compo, 1998). In previous studies,

the wavelet analysis of electric field was made to show return strokes spectrum in the time domain (e.g. Miranda, 2008). Sharma et al. (2011) used WT to analyze different lightning events, such as negative and positive return strokes, PB (Preliminary Breakdown) pulses, stepped leaders and so on. Li et al. (2013) found that the Laplace wavelet had a greater accuracy in determining the time and frequency of the electromagnetic field of first and subsequent return strokes. Esa et al. (2014) investigated the wavelet characteristics of the first electric field pulse of four different flash types including negative cloud-to-ground flash (−CG), positive cloud-to-ground flash (+CG), cloud flash (IC) and isolated breakdown flash (IB).

In this paper, the magnetic-field signals recorded by Nanjing Lightning Location Network were analyzed by WPT (Wavelet Packet Transform) to obtain wavelet packet energy spectra of three kinds of lightning events (cloud pulse, return stroke and stepped leader). Based on the wavelet packet energy spectra of different events, the average energy percentage of each frequency for different events were given. Three indices were proposed to distinguish different lightning events and evaluated the recognition accuracy.

2 Instrumentation

Fig. **1** shows the geographical layout of the Nanjing Lightning Location Network. There are seven detection stations in Nanjing and its surrounding areas. This network has a baseline of about 18 to 48 kilometers and can detect total lightnings in three-dimension. Each station is mainly composed of two orthogonal low-frequency magnetic antennas, a high-speed data acquisition system and a high-precision GPS clock. The most basic part of the magnetic antenna is the loop coil wound on a magnetic rod. According to Faraday law of electromagnetic induction, when the magnetic lines pass through the loop coil, it would inevitably generate the induced electromotive force on the loop. The magnetic antenna detects the induced signal to realize signal detection and reception (Liu et al., 2019). The bandwidth of the magnetic antenna ranges from approximately 10 kHz to 300 kHz and the frequency response curve is shown in Fig. 2. The high-speed data acquisition system uses the trigger acquisition method to continuously and synchronously collect, record, store and transmit the real lightning pulse signal, in which the signal sampling rate is 1 MS/s. The time synchronization between different detection stations is achieved by a high-precision GPS clock with a time accuracy of 50 ns.

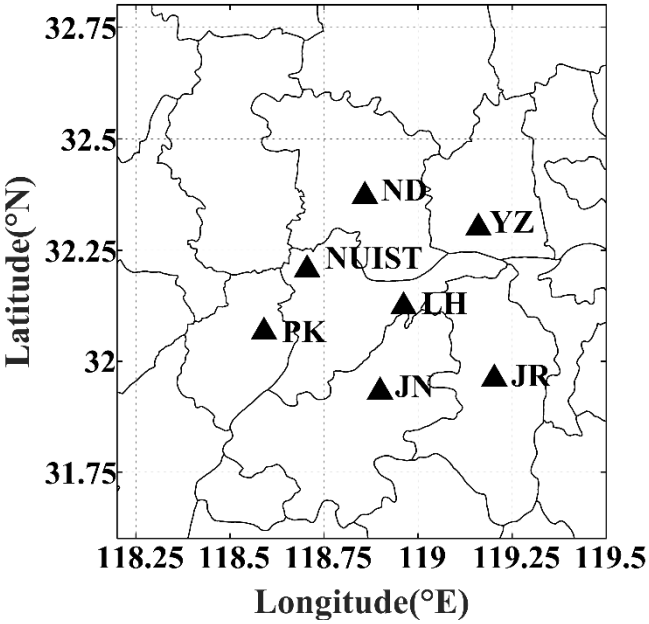

Fig. 1. Geographical layout of the Nanjing Lightning Location Network. Detection Stations are represented by black triangles.

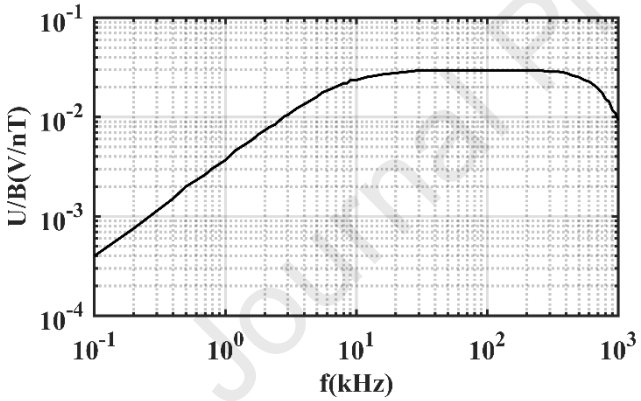

Fig. 2. The frequency response curve of the low-frequency magnetic antenna.

3 Methodology

3.1 Wavelet Theory

Lightning is a non-stationary signal with many characteristics such as abrupt changes and trends. These characteristics are important both scientifically, to understand the physics of the discharge, and practically, to distinguish different lightning events. In order to understand the temporal features of different lightning events, the WT has been used in this paper. Since the WT and its mathematical description have been detailed in many previous studies, we just present a brief introduction of WT in this paper.

The FT technique decomposes a signal based on the infinite functions of sine and cosine waves, yet the wavelet technique decomposes a signal in a space whose base can be orthogonal or

nonorthogonal functions but finite functions. These functions are called mother wavelets ($\psi(t)$). There are various mother wavelets, such as Haar wavelet, Daubechies wavelet, Morlet wavelet, Meyer wavelet, and so on. The Daubechies wavelets are the most widely used tightly supported orthogonal real wavelets, which have outstanding time-frequency analysis capabilities and signal mutation detection capabilities, so db16 wavelet was chosen in this paper. The expanded ($\psi(at)$) and translated ($\psi(t+\tau)$) version of a mother wavelet is called daughter wavelet. The WT can be considered as computing the similarity between the original signal and daughter wavelets. The WT of a continuous time series $x(t)$ is

$$WT(a,\tau) = \frac{1}{\sqrt{a}} \int_{-\infty}^{+\infty} x(t) * \psi(\frac{t-\tau}{a}) dt \quad (1)$$

where $1/\sqrt{a}$ is a normalization factor, τ is the translation parameter in time space and a is the scale parameter that is related to the frequency of a signal. The (*) indicates the inner product.

In addition, the WT is divided into the continuous wavelet transform (CWT) and the discrete wavelet transform (DWT). The CWT generates computational redundancy that requires a huge amount of computational space and time. However, the DWT provides plenty and effective information both for analysis and reconstruction of the original signal, with much efficient computing capacity. Furthermore, the DWT is extremely easier to employ compared to the CWT. Therefore, we choose DWT in this paper.

3.2 Wavelet Packet Decomposition

According to the signal decomposition theory, a signal is decomposed into cA (approximation coefficients) by a low-pass filter and cD (detail coefficients) by a high-pass filter. Only the approximate part is decomposed iteratively in DWT (Mallat, 1989) which makes it suffer from a relatively low resolution in the high-frequency part. The WPT, in comparison, further decomposes both the approximate part and the detailed part of the signal (Gao and Yan, 2006). Computation of wavelet packet decomposition was done by Matlab. Fig. 3 shows the three-layer wavelet packet decomposition process which produces a total of eight frequency sub-bands. If the sampling rate of the original signal is *fs* Hz, the highest frequency is *fs/2* Hz according to the Nyquist theorem. Therefore, in the first layer, the frequency sub-band between 0 and *fs/4* is captured in the approximation component and the frequency sub-band between *fs/4* and *fs/2* is captured in the detail component. In summary, if a signal is decomposed by *N*-layer wavelet packet, it could be divided into 2^N frequency sub-bands. And the frequency range of the j^{th}sub-band is$(fs/2^{N+1}) \times j \sim (fs/2^{N+1}) \times (j+1)$, where$j = 0,1,2,\cdots,2^N - 1$.

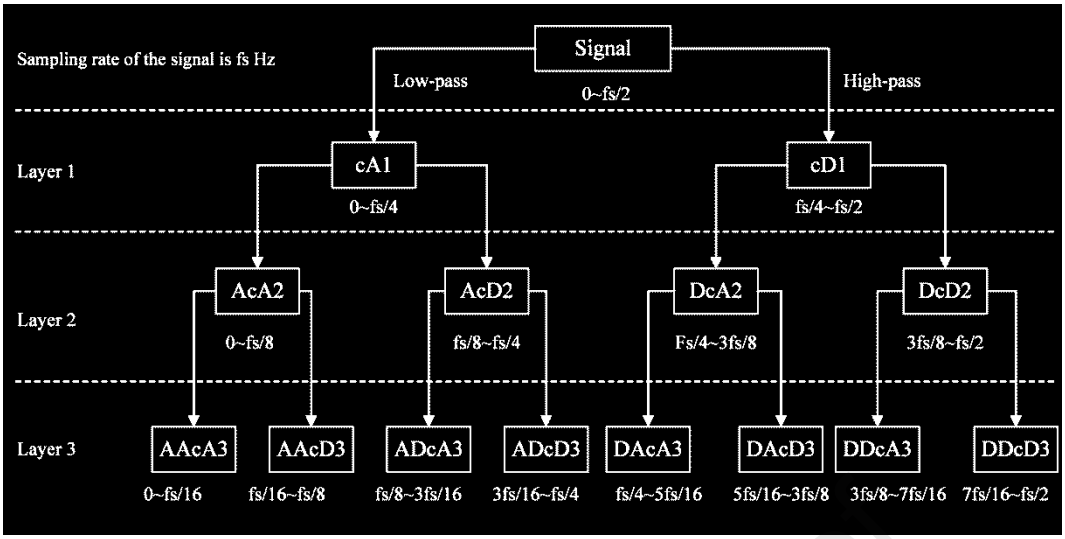

Fig. 3. Three-layer wavelet packet decomposition tree and corresponding frequency sub-bands.

In addition, the number of decomposition layers (*N*) could be calculated as follows:

$$N = floor(log_2\left(\frac{fs}{fc}\right) - 1) \tag{2}$$

where *fs* is the sampling frequency and *fc* is determined by the required lowest frequency range. And *floor* is a function that gets the inferior integer part of the value. In this paper, the sampling frequency *fs* is 1 MHz and *fc* is 1.5 kHz, thus the number of decomposition layer (*N*) is eight.

3.3 Wavelet Packet Energy Spectra

The signal *x(t)* is decomposed by *N*-layer wavelet packet and then the wavelet packet decomposition sequence $S_{Nj}(j = 0,1,2,\cdots,2^N - 1)$ could be obtained. The energy spectrum of j^{th} frequency sub-band for N^{th} layer is $E_{Nj} = \left|u_{Nj}\right|^2$, where u_{Nj} is the amplitude of discrete points for S_{Nj} and j is the sequence number of frequency sub-band for *N*-layer wavelet packet decomposition (Li and Goldstein, 1990). Therefore, the energy spectrum of *N*-layer wavelet packet decomposition is

$$E_N = \left[E_{N,0}, E_{N,1}, E_{N,2}, \cdots, E_{N,2^{N-1}}\right]^T \tag{3}$$

4 Results and Discussion

4.1 Wavelet Packet Energy Spectra of Different Lightning Events

Firstly, the magnetic-field data of three typical lightning events recorded by Nanjing Lightning Location Network in 2018 were analyzed by WPT to show the time-frequency features of different lightning events. Fig. 4a shows the magnetic-filed waveform of a lightning flash including three typical lightning events and Fig. 4b shows the variation of located heights with time. The location results were computed by 3-D time of arrival (TOA) method. According to the

location results, the typical magnetic-field waveforms of three events are selected as shown in the rectangular dotted frames of Fig. 4a. The first rectangular dotted frame includes a cloud pulse event and the second rectangular dotted frame includes a return stroke and its corresponding stepped leaders. The magnetic field data of these three events and their corresponding wavelet packet energy spectra are respectively shown in Fig. 5, Fig. 6 and Fig. 7. Plot (a) of these three figures shows the time domain magnetic-field data for different events and plot (b) shows the corresponding wavelet packet energy spectra that provide the energy distribution in time-frequency domain. Plot (c) depicts the sum of energy of the entire time window for each frequency. In other words, plot (c) provides the energy distribution in frequency domain. In all these figures, the horizontal axes of plot (a) and (b) represent time at microsecond scale and that of plot (c) represent energy. The vertical axes of plot (a) represent the magnetic field intensity and that of plot (b) and (c) represent the frequency. The strength of the energy spectra is indicated by the color bars.

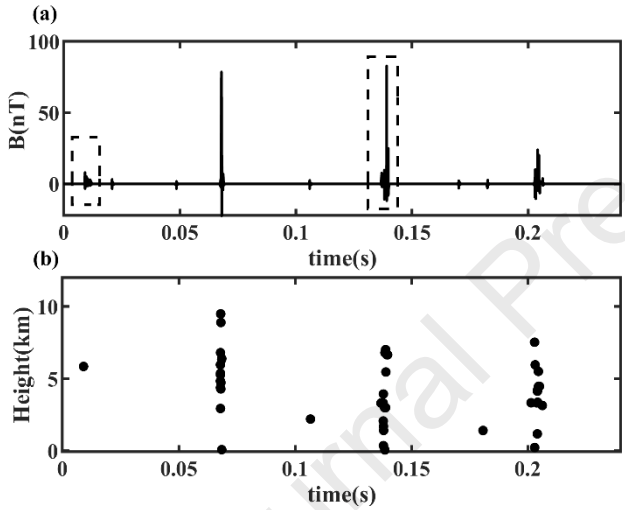

Fig. 4. Magnetic-filed waveform and location results for a lightning flash. (a) Magnetic-filed waveform. (b) Height-time plot.

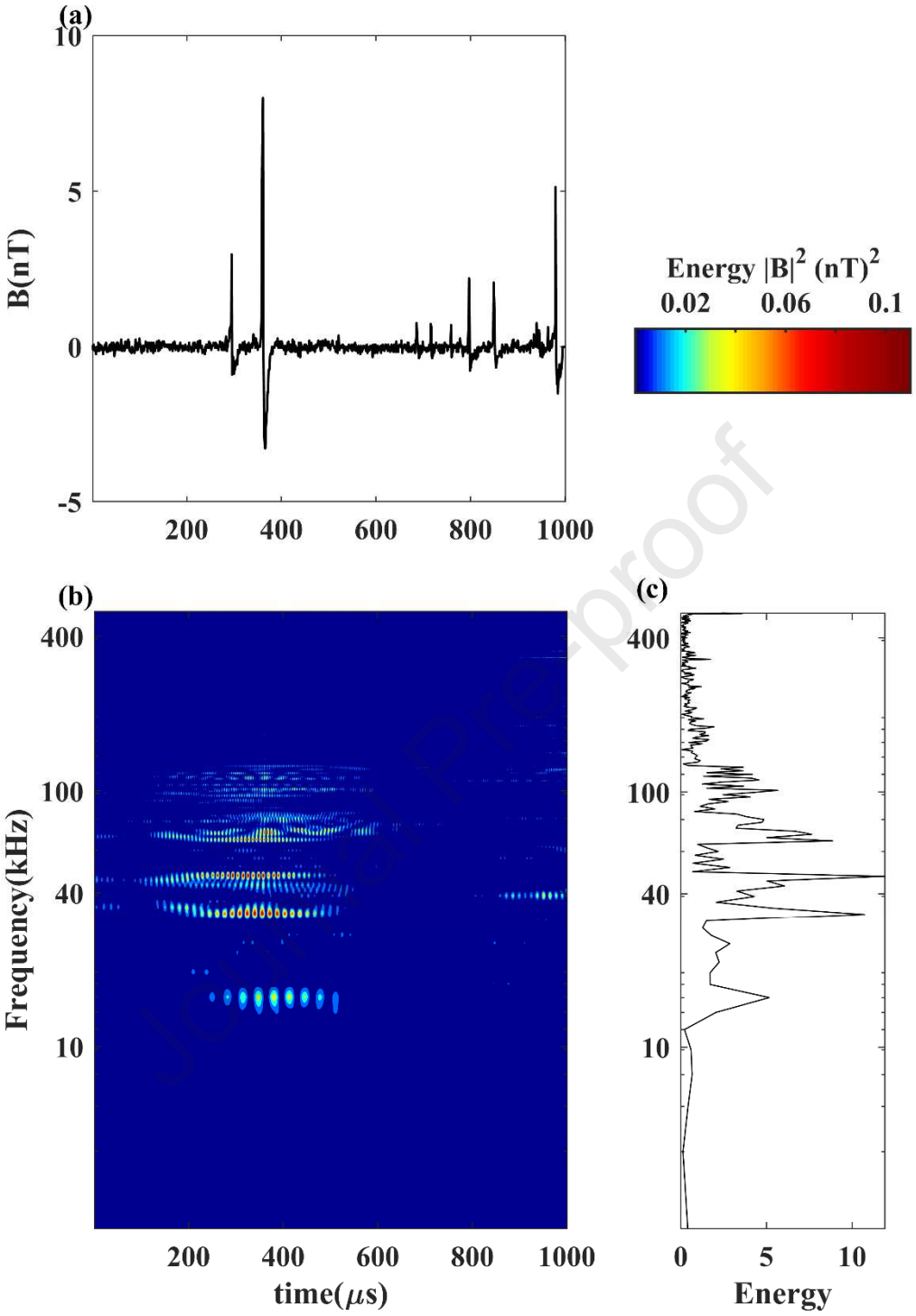

Fig. 5. Magnetic-filed waveform and its wavelet packet energy spectrum of cloud pulse corresponding to the first rectangular dotted frame in **Fig. 4**a. (a) Magnetic-filed waveform. (b) Wavelet packet energy spectrum. (c) The sum of energy of the entire time window for each frequency.

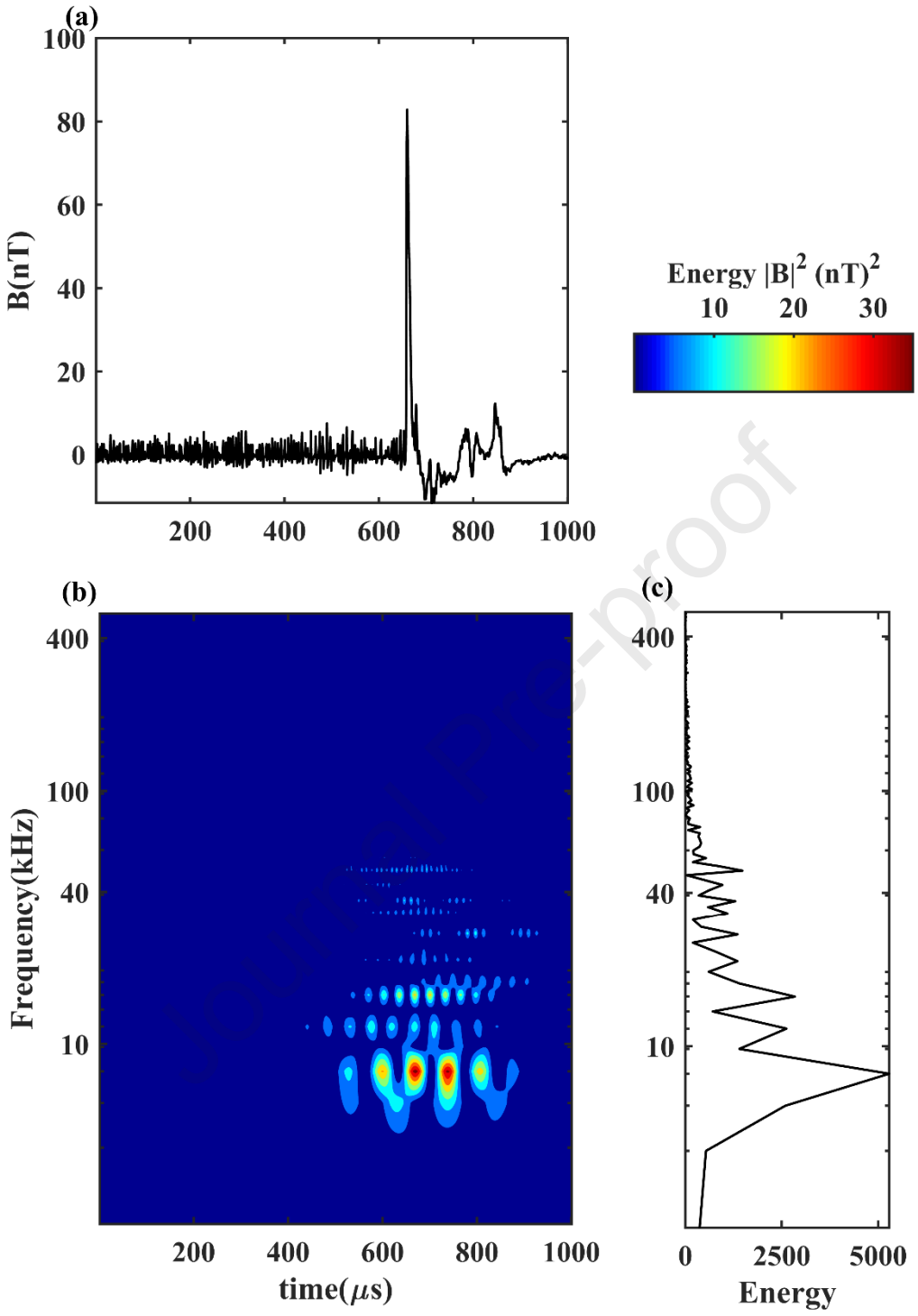

Fig. 6. Magnetic-filed waveform and its wavelet packet energy spectrum of a return stroke corresponding to the second rectangular dotted frame in Fig. 4a.

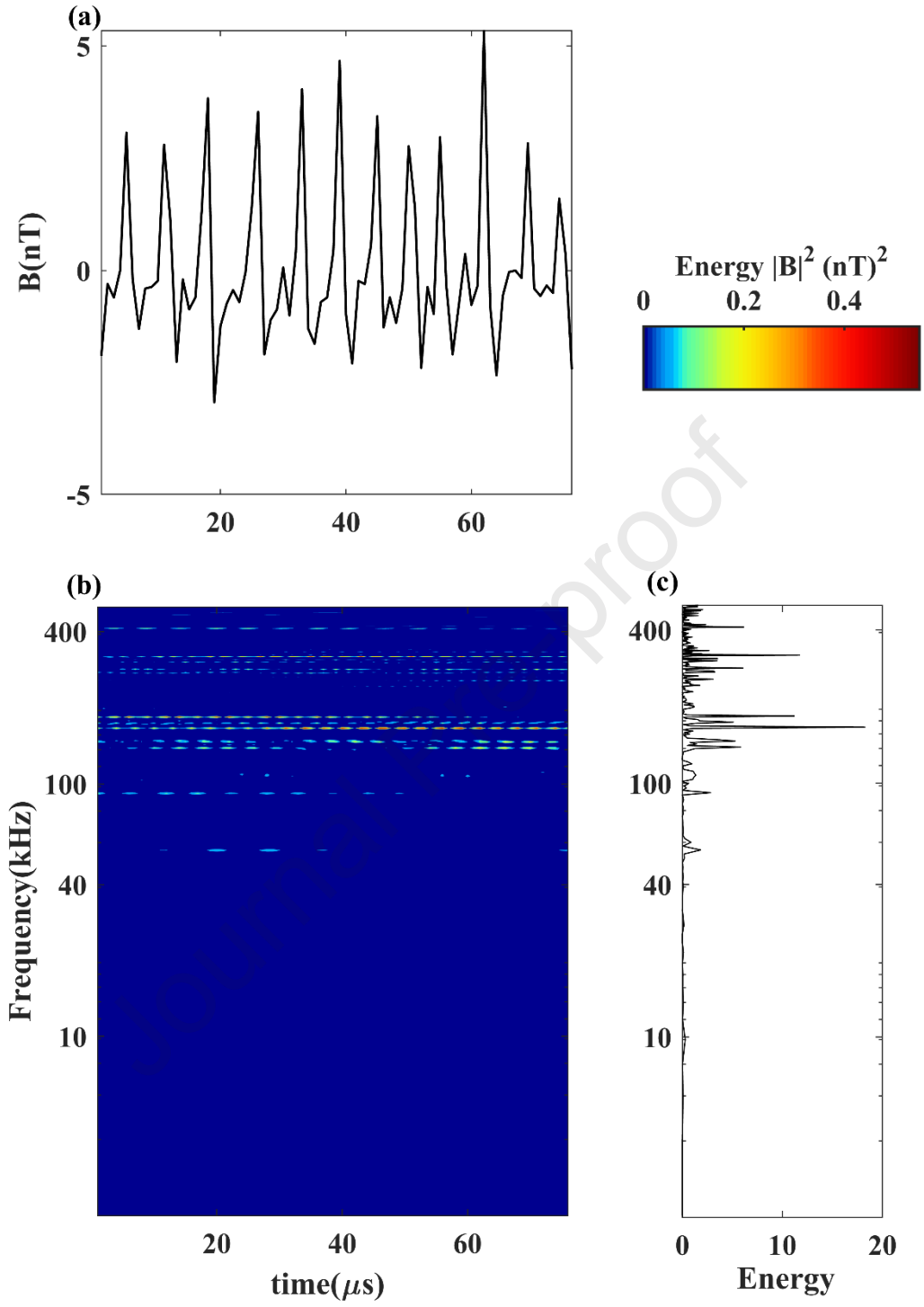

Fig. 7. Magnetic-filed waveform and its wavelet packet energy spectrum of stepped leaders corresponding to the return stroke in Fig. 6.

Fig. **5** depicts the magnetic field waveform of cloud pulses with the window size of 1000 μs and its corresponding wavelet energy spectrum. This event corresponds to the first rectangular dotted frame in Fig. 4a. In Fig. 5, it is clearly shown that pulses in the clouds predominantly radiated in the frequency range 13~137 kHz. The maximum energy radiated by the largest pulse is

approximately 0.119 nT^2. Fig. **6** shows the magnetic field waveform of the return stroke with window size of 1000 μs, which corresponds to the second rectangular dotted frame in Fig. 4a. As seen in Fig. 6, the maximum energy is 37.22 nT^2 and the spectrum of the return stroke mainly lies below 15 kHz, this is contrary of what is known from Fourier analysis, which indicates the energy of a return stroke radiates not at a particular frequency but over a range of frequencies. Fig. **7** shows wavelet packet energy spectra of stepped leaders corresponding to the return stroke in Fig. 6. It is seen in Fig. 7 that the spectral range of this event is found between 138 and 400 kHz. In addition, the maximum energy is about 0.55 nT^2.

In this work, the range of frequency in which the predominant energy is radiated, is termed as spectral range. According to Fig. 5, Fig. 6 and Fig. 7, it is noted that the spectral ranges of these three events are much different and that of return strokes are lower than other two events. In addition, it is found that the energy radiated by the cloud pulses and stepped leaders are much smaller than that of the return strokes. It reveals that the return strokes are the strongest source of energy at lower frequencies. What is more, it is obvious that the spectral range of the stepped leader is higher than that of the cloud pulse.

Then, 232 cloud pulses, 876 return strokes and 373 stepped leaders are analyzed to get the average spectral range of these three lightning events. As we can see in Table 1, the cloud pulses are found to radiate predominantly in the average spectral range 9~56 kHz with a minimum value of 2 kHz to a maximum value of 414 kHz. The return strokes are found to predominantly radiate in the average spectral range 2~14 kHz with a minimum value of 2 kHz to a maximum value of 238 kHz. In addition, the spectral distribution of the stepped leaders lies between 2 and 500 kHz with an average spectral range of 52~236 kHz.

Table 1. Statistics of the average spectral range of cloud pulse, return stroke and stepped leader.

	Spectral range(kHz)		
	Minimum	Maximum	Average range
Cloud pulse	2	414	9~56
Return stroke	2	238	2~14
Stepped leader	2	500	52~236

4.2 Proposed Identification Indices

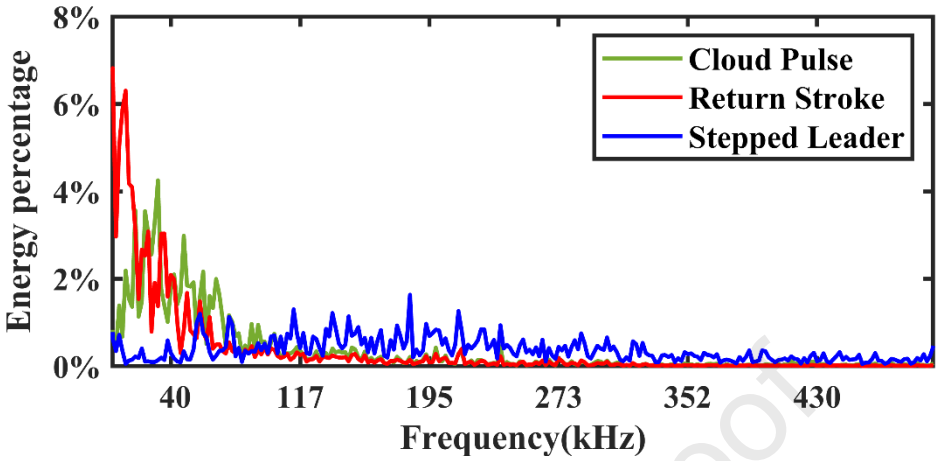

Fig. 8. The average energy percentage of each frequency for three kinds of lightning events.

In this section, 232 cloud pulses, 876 return strokes and 373 stepped leaders are analyzed by WPT to get the energy distribution features of different lightning events in frequency domain. As shown in section 3.2 and section 4.1, a signal could be decomposed into different frequency components by WPT and the energy radiated by each frequency component is different. In this work, the energy percentage is defined as the ratio of the energy radiated by each frequency component to the total energy of all frequency components. Fig. **8** shows the average energy percentage of each frequency for three kinds of lightning events. It is clearly seen that the energy percentage of return stroke shows a decreasing trend below 20 kHz, whereas the energy percentage of cloud pulses increase in the same frequency range. In addition, the energy radiated by stepped leader is particularly weak below 80 kHz compared to other two events. According to Fig. 8, the following three indices are proposed to discriminate these three kinds of events:

$$K1 = \left(\frac{\sum_{f=4}^{100} E_f}{EE} - \frac{\sum_{f=102}^{198} E_f}{EE}\right) \times 100 \quad (4)$$

$$K2 = \left(\frac{\sum_{f=4}^{20} E_f}{EE} - \frac{\sum_{f=22}^{38} E_f}{EE}\right) \times 100 \quad (5)$$

$$K3 = \left(\frac{\sum_{f=4}^{80} E_f}{EE}\right) \times 100 \quad (6)$$

Where E_f is the energy corresponding to the specific frequency f and it is calculated by WPT. EE is the total energy of all frequency components.

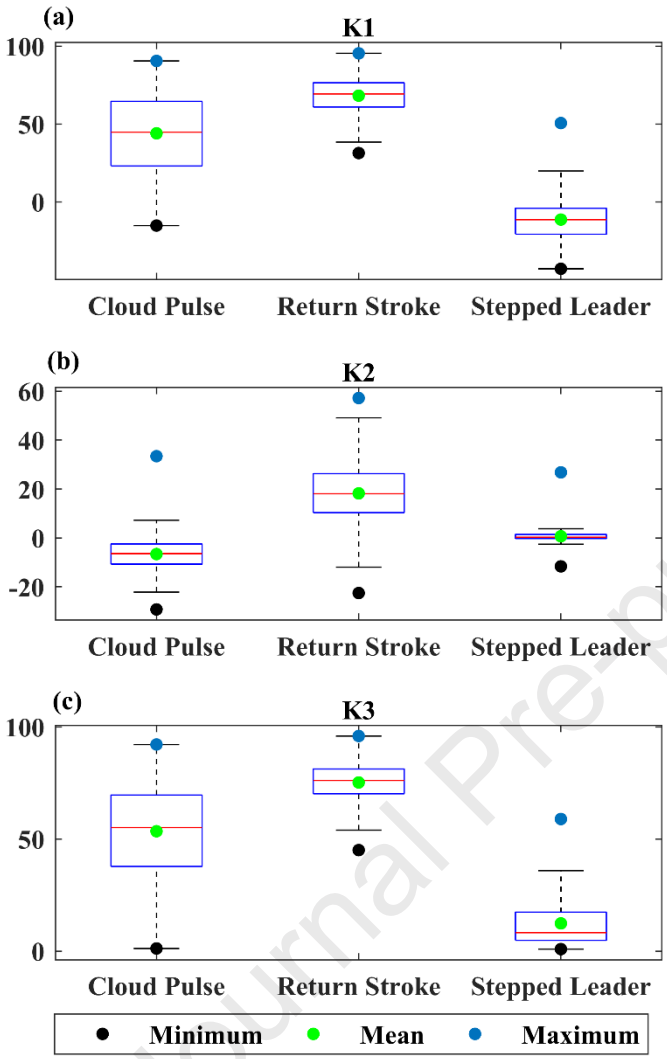

Fig. 9. Data distribution of three indices ((a)*K1*, (b)*K2*, (c)*K3*) given by box plots. Black, green and blue dots represent minimum, mean and maximum of indices for different lightning events, respectively.

Fig. **9** shows the data distribution of the three indices for the three different lightning events using box plots. In Fig. 9, plot (a), (b)and (c) respectively provide the data distribution of *K1*, *K2* and *K3* for different events. In these plots, the horizontal axes represent different events and the vertical axes represent values of *K1*, *K2* and *K3*. As seen in the figure, the dominant distribution intervals (blue rectangles) of three indices for different events are different. For *K1*, the dominant distribution intervals of the cloud pulse, the return stroke and stepped leader are 23.03~64.51, 60.90~76.48, -20.79~-4.12, respectively. For *K2*, the dominant distribution intervals of the cloud pulse, the return stroke and stepped leader are -10.72~-2.46, 10.34~26.24, -0.26~1.42, respectively. For *K3*, the dominant distribution intervals of the cloud pulse, the return stroke and stepped leader are 37.78~69.61, 70.21~81.21, 4.85~17.38, respectively. Considering sampling randomness of signals and the data dispersity of indices, the values of these three indices are given as follows:

1) Cloud pulses: $K1 > 0$ & $K2 < 0$ & $K3 > 20$

2) Return stroke: $K1 > 0$ & $K2 > 0$ & $K3 > 50$

3) Stepped leader: $K1 < 10$ & $K2 < 10$ & $K3 < 30$

And then, 100 cloud pulses, 100 return strokes and 100 stepped leaders are randomly selected to show recognition accuracy of three proposed indices. For a specific lightning event, recognition rate refers to the ratio of the number of accurately identified cases to the total number of this kind of event. And false-recognition rate is the ratio of the number of cases that are recognized as other two types to the total number of this kind of event. Unrecognized rate is the ratio of the number of cases that could not be recognized as one of these three types to the total number of this kind of event. As shown in Table 2, the proposed indices can properly identify different lightning events with recognition rates 80%, 91% and 93% for the cloud pulse, return stroke and stepped leader, respectively. Additionally, the return stroke has the lowest unrecognized rate and the stepped leader has the lowest false-recognition rate.

Table 2. The identification results of 300 randomly selected cases (100 cloud pulses, 100 return strokes and 100 stepped leaders) obtained using three indices.

	Cloud pulses	Return stroke	Stepped leader
Recognition rate	80%	91%	93%
False-recognition rate	11%	8%	2%
Unrecognized rate	9%	1%	5%

4.3 The Flowchart of a New Real-Time Identification Method

As verified in section 4.2, three proposed indices could effectively distinguish different lightning events. Additionally, it is known that the DWT allows efficient calculation and can save computational space and time. Based on these facts, a new real-time identification method is proposed in this paper.

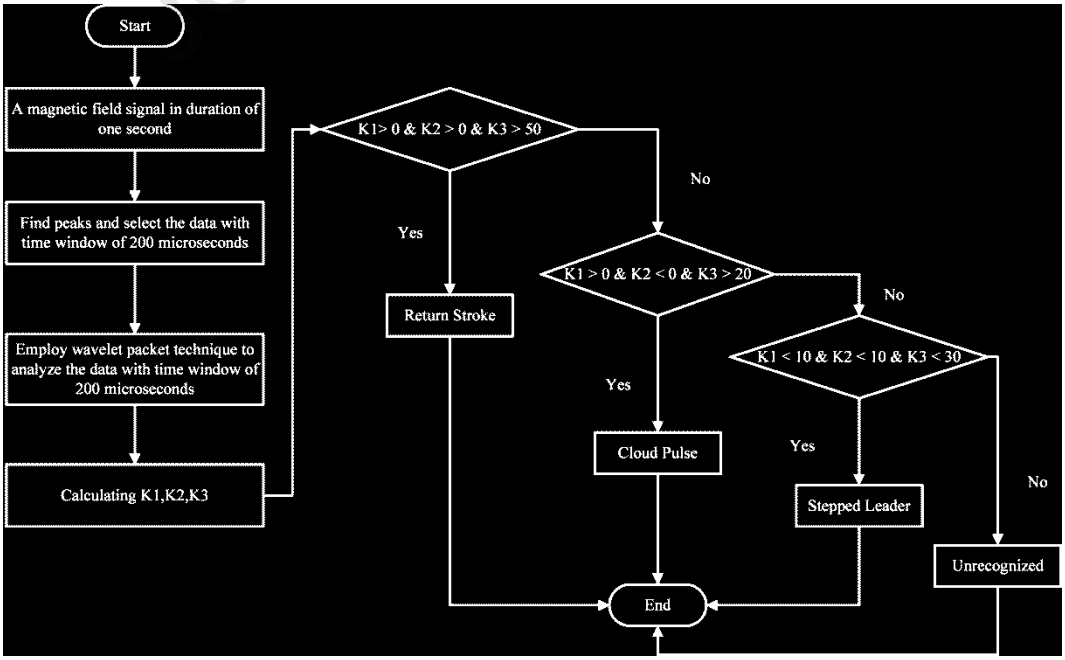

Fig. 10. Flowchart of the proposed identification method.

Fig. **10** shows the flowchart of this new real-time identification method. This proposed method is described in detail as follows: (1) As mentioned in section 2, our high-speed data acquisition system collects lightning pulse signals, in which the sampling rate is 1 MS/s and the length of each signal is one second. (2) Then, many peaks of this one second signal could be found in basis of some restrictions. The data with time window of 200 μs centered on these peaks would be selected from this one second signal. Noted that this window length is sufficient to cover much information of each record. (3) The selected magnetic-field data would be computed by WPT and the wavelet energy spectra could be attained. (4) Finally, we can distinguish different events based on *K1*, *K2* and *K3* that shown in section 4.2.

5 Conclusion

This study proposes a new recognition method for lightning pulses. The energy features of three kinds of lightning events (cloud pulse, return stroke and stepped leader) are analyzed by WPT. Firstly, the wavelet spectra of three typical lightning events are given and it is found that spectral ranges of these three events are much different. The statistical results of 232 cloud pulses, 876 return strokes and 373 stepped leaders indicate that the average spectral ranges are 9~56 kHz, 2~14 kHz and 52~236 kHz, respectively. It is clear that the predominant radiation frequency of the stepped leader is the highest and that of the return strokes is the lowest. According to the average energy percentage of each frequency for different events that is shown in Fig. 8, three indices are proposed to distinguish different lightning events, and then the validity of the three indices are evaluated. The result shows that the recognition rates of the cloud pulse and the return stroke are respectively 80% and 91% and that of stepped leader is up to 93%. Based on these three indices, a new real-time identification method is proposed in this paper and the flowchart of it is given.

The results shown in this study are helpful to improve our understanding on the properties of energy and frequencies of different lightning events in Nanjing, which is important to the protection of electric equipment from damages caused by the indirect impacts of lightning. The new recognition method is helpful to distinguish cloud pulse, return stroke and stepped leader, thus can be used to analyze the development of lightning, especially in a statistical way. Note the results are obtained based on the measurements in Nanjing, however, lightning properties vary geographically, and are affected by ambient conditions such as vapor source and aerosols. Therefore, more measurements are needed in the future to better understand the radiation energy and frequencies of lightning, and to develop a more statistically robust recognition approach, which may include information of geolocation and ambient conditions, to identify different lightning events.

Acknowledgement

This work was supported by National Key R&D Program of China [grant number: 2017YFC1501505], the National Natural Science Foundation of China [grant number: 41775006, 41905124], and Natural Science Foundation of Jiangsu Province, China [grant number: BK20190778].

Reference

[1] Miranda, F. J. D. , Pinto, O. , & Saba, M. M. F. . (2003). A study of the time interval between return strokes and k-changes of negative cloud-to-ground lightning flashes in brazil. *Journal of Atmospheric and Solar-Terrestrial Physics, 65*(3), 293-297.

[2] Maggio, C. R. , Marshall, T. C. , & Stolzenburg, M. . (2009). Estimations of charge transferred and energy released by lightning flashes. *Journal of Geophysical Research Atmospheres, 114*(D14).

[3] Dwyer, J. R. , & Uman, M. A. . (2014). The physics of lightning. *Physics Reports, 534*(4), 147-241.

[4] Xiushu Qie, Qinlin Zhang, & Tie Yuan. 2013. Physics of lightning. *Science Press*.

[5] Weidman, C. D. , & Krider, E. P. . (1986). The amplitude spectra of lightning radiation fields in the interval from 1 to 20 mhz. *Radio Science, 21*(6), 964-970.

[6] Salimi, B. , Mehranzamir, K. , & Abdul-Malek, Z. . (2013). Statistical analysis of lightning electric field measured under equatorial region condition. *Procedia Technology, 11*, 525-531.

[7] Le Vine, D.M.. (1987). Review of measurements of the RF spectrum of radiation from lightning. *Meteorology and Atmospheric Physics, 37*(3), 195-204.

[8] Willett, J. C. , Bailey, J. C. , Leteinturier, C. , & Krider, E. P. . (1990). Lightning electromagnetic radiation field spectra in the interval from 0.2 to 20 mhz. *Journal of Geophysical Research Atmospheres, 95*(D12).

[9] Watt, A.D. & Maxwell, E.L.. (1957). Characteristics of Atmospheric Noise from 1 to 100 KC. *Proceedings of the IRE. 45*(6), 787 - 794. 10.1109/JRPROC.1957.278476.

[10] Serhan, G. I. , Uman, M. A. , Childers, D. G. , & Lin, Y. T. . (1980). The rf spectra of first and subsequent lightning return strokes in the 1- to 200-km range. *Radio Science, 15*(6), 1089-1094.

[11] Issac, M. , Renuka, G. , & Venugopal, C. . (2004). Wavelet analysis of long period oscillations in geomagnetic field over the magnetic equator. *Journal of Atmospheric and Solar-Terrestrial Physics, 66*(11), 919-925.

[12] Torrence, C., Compo, G.P. . (1998). A practical guide to wavelet analysis. *Bulletin of the American Meteorological Society, 79*, 61–78.

[13] Miranda, F. J. . (2008). Wavelet analysis of lightning return stroke. *Journal of Atmospheric and Solar-Terrestrial Physics,70*(11-12), 1401-1407.

[14] Sharma, S. R. , Cooray, V. , Fernando, M. , & Miranda, F. J. . (2011). Temporal features of different lightning events revealed from wavelet transform. *Journal of Atmospheric and Solar-Terrestrial Physics, 73*(4), 507-515.

[15] Li, Q. , Li, K. , & Chen, X. . (2013). Research on lightning electromagnetic fields associated with first and subsequent return strokes based on laplace wavelet. *Journal of Atmospheric and Solar-Terrestrial Physics, 93*, 1-10.

[16] Esa, M. R. M. , Ahmad, M. R. , & Cooray, V. . (2014). Wavelet analysis of the first electric field pulse of lightning flashes in Sweden. *Atmospheric Research, 138*, 253-267.

[17] Liu Chao, Wang Lei, Zhou Maokun, Yu Zhenguo, Peng Xiaoyu & Hou Wenhao, et al. . (2019). Design and Application of Lightning Monitoring Circuit Based on Low Frequency Magnetic Antenna. *Insulators and Surge Arresters, 000*(003), 10-18.

[18] Mallat, S.G. . (1989). A theory for multiresolution signal decomposition: the wavelet representation. *IEEE Transactions on Pattern Analysis and Machine Intelligence 11* (7), 674-693.10.1109/34.192463.

[19] Gao, R. X. , & Yan, R. . (2006). Non-stationary signal processing for bearing health monitoring. *International Journal of Manufacturing Research, 1*(1), 18.

[20] Li, F. K. , & Goldstein, R. M. . (1990). Studies of multibaseline spaceborne interferometric synthetic aperture radars. *IEEE Transactions on Geoscience and Remote Sensing*, *28*(1), 88-97.

Highlights

1. The magnetic field data were recorded by Nanjing Lightning Location Network.
2. The wavelet packet transform was used to analyze lightning magnetic-field signals in order to obtain the predominant frequency range of different lightning events.
3. Finding that the energy variation in frequency domain is different for different lightning events.
4. Based on the wavelet packet transform, three new identification indices were proposed to distinguish cloud pulse, return stroke and stepped leader.

Declaration of interests

☒ The authors declare that they have no known competing financial interests or personal relationships that could have appeared to influence the work reported in this paper.

☐The authors declare the following financial interests/personal relationships which may be considered as potential competing interests: